





The following article appeared in AIP Advances 8, 056434 (2018); and may be found at: <https://doi.org/10.1063/1.5006467>

All article content, except where otherwise noted, is licensed under a Creative Commons Attribution 4.0 International (CC BY 4.0) license <http://creativecommons.org/licenses/by/4.0/>

Magnetostructural transitions and magnetocaloric effects in $\text{Ni}_{50}\text{Mn}_{35}\text{In}_{14.25}\text{B}_{0.75}$ ribbons

Cite as: AIP Advances **8**, 056434 (2018); <https://doi.org/10.1063/1.5006467>

Submitted: 25 September 2017 . Accepted: 04 December 2017 . Published Online: 12 January 2018

Sudip Pandey , Abdiel Quetz , P. J. Ibarra-Gaytan, C. F. Sánchez-Valdés , Anil Aryal, Igor Dubenko, Jose Luis Sanchez Llamazares , Shane Stadler, and Naushad Ali



View Online



Export Citation



CrossMark

ARTICLES YOU MAY BE INTERESTED IN

[Effect of Bi substitution on the magnetic and magnetocaloric properties of \$\text{Ni}_{50}\text{Mn}_{35}\text{In}_{15-x}\text{Bi}_x\$ Heusler alloys](#)

AIP Advances **8**, 056409 (2018); <https://doi.org/10.1063/1.5004694>

[Magnetic and magnetocaloric properties of Ni-Mn-Cr-Sn Heusler alloys under the effects of hydrostatic pressure](#)

AIP Advances **8**, 056408 (2018); <https://doi.org/10.1063/1.5005802>

[Microstructure, magnetic and magnetocaloric properties in \$\text{Ni}_{42.9}\text{Co}_{6.9}\text{Mn}_{38.3}\text{Sn}_{11.9}\$ alloy ribbons](#)

AIP Advances **8**, 056410 (2018); <https://doi.org/10.1063/1.5006245>

Don't let your writing
keep you from getting
published!

AIP | Author Services

Learn more today!

Magnetostructural transitions and magnetocaloric effects in $\text{Ni}_{50}\text{Mn}_{35}\text{In}_{14.25}\text{B}_{0.75}$ ribbons

Sudip Pandey,^{1,a} Abdiel Quetz,¹ P. J. Ibarra-Gaytan,² C. F. Sánchez-Valdés,³ Anil Aryal,¹ Igor Dubenko,¹ Jose Luis Sanchez Llamazares,^{2,a} Shane Stadler,⁴ and Naushad Ali¹

¹*Department of Physics, Southern Illinois University, Carbondale, IL 62901, USA*

²*Instituto Potosino de Investigación Científica y Tecnológica A.C., Camino a la Presa San Jose 2055, Col. Lomas 4^a sección, San Luis Potosí, S.L.P. 78216, Mexico*

³*División Multidisciplinaria, Ciudad Universitaria, Universidad Autónoma de Ciudad Juárez (UACJ), calle José de Jesús Macías Delgado # 18100, Ciudad Juárez 32579, Chihuahua, México*

⁴*Department of Physics & Astronomy, Louisiana State University, Baton Rouge, LA 70803, USA*

(Presented 8 November 2017; received 25 September 2017; accepted 4 December 2017; published online 12 January 2018)

The structural, thermal, and magnetic behaviors, as well as the martensitic phase transformation and related magnetocaloric response of $\text{Ni}_{50}\text{Mn}_{35}\text{In}_{14.25}\text{B}_{0.75}$ annealed ribbons have been investigated using room-temperature X-ray diffraction (XRD), differential scanning calorimetry (DSC), and magnetization measurements. $\text{Ni}_{50}\text{Mn}_{35}\text{In}_{14.25}\text{B}_{0.75}$ annealed ribbons show a sharper change in magnetization at the martensitic transition, resulting in larger magnetic entropy changes in comparison to bulk $\text{Ni}_{50}\text{Mn}_{35}\text{In}_{14.25}\text{B}_{0.75}$. A drastic shift in the martensitic transformation temperature (T_M) of 70 K to higher temperature was observed for the annealed ribbons relative to that of the bulk ($T_M = 240$ K). The results obtained for magnetic, thermal, structural, and magnetocaloric properties of annealed ribbons have been compared to those of the corresponding bulk alloys. © 2018 Author(s). All article content, except where otherwise noted, is licensed under a Creative Commons Attribution (CC BY) license (<http://creativecommons.org/licenses/by/4.0/>). <https://doi.org/10.1063/1.5006467>

INTRODUCTION

The off-stoichiometric Ni-Mn-In Heusler systems have been drawing interest due to their temperature-induced magnetostructural transitions (MST), which are responsible for extreme physical properties like giant normal and inverse magnetocaloric effects,^{1–3} giant magnetoresistance,^{4,5} large anomalous Hall effects,⁶ and magnetic shape memory effects.⁷ Most of the research for the Ni-Mn-In based Heusler alloys have been being carried out for bulk materials by means of conventional melting techniques followed by lengthy high-temperature thermal annealing.^{8–10} Currently, a variety of magnetocaloric materials have been successfully synthesized in the form of ribbons by rapid quenching using the melt-spinning technique.^{11–15} It has been observed that single-phase homogeneous polycrystalline materials are formed in melt-spun ribbons, avoiding the need for long-term thermal annealing of their bulk counterparts.^{13,16} In addition, previous studies indicate that if synthesis condition are properly controlled, ribbons produced by melt spinning techniques may have a highly textured microstructure and negligible demagnetization field along the ribbon length.^{17,18} It has been reported that melt-spinning effectively promotes more homogeneous materials, and reduces the annealing time with improved MCE properties.^{12,15,19}

In recent studies, we have reported on the magnetostructural, magnetic, magnetocaloric, and magnetoresistance properties of bulk Ni-Mn-In-B based systems.^{20–22} The objective of the current

^aCorresponding author: e-mail: sudip@siu.edu (Sudip Pandey) jose.sanchez@ipicyt.edu.mx (J. L. Sánchez Llamazares)



research is to fabricate ribbons by rapid solidification using the melt-spinning technique and to study the magnetic, thermal, structural, and magnetocaloric properties of $\text{Ni}_{50}\text{Mn}_{35}\text{In}_{14.25}\text{B}_{0.75}$ annealed ribbons and to compare these properties to those of the corresponding bulk alloys.

MATERIALS AND METHODS

A $\text{Ni}_{50}\text{Mn}_{35}\text{In}_{14.5}\text{B}_{0.75}$ ingot of nominal composition was prepared by arc-melting 4N purity elements Ni, Mn, In, and B in a high-purity argon atmosphere. The ingot was re-melted several times to ensure the homogeneity. From the sample obtained by arc-melting, rapidly solidified ribbons (with thicknesses $\approx 30\text{--}35\ \mu\text{m}$) of $\text{Ni}_{50}\text{Mn}_{35}\text{In}_{14.5}\text{B}_{0.75}$ nominal composition (same as bulk) were produced at a linear speed $v = 20\ \text{m/s}$ using an Edmund Buhler model SC melt spinner system in a high purity argon atmosphere. As-solidified melt-spun ribbons were sealed in a quartz ampoule under a highly pure Ar atmosphere and annealed at 1073 K for 10 minutes. Water quenching followed annealing. The crystal structures and phase purity of the as-solidified sample were studied using a high resolution Rigaku Smartlab diffractometer employing $\text{Cu-K}\alpha$ radiation. The pattern was measured on finely powdered sample. The structural phase transformations of the ribbons were studied using a differential scanning calorimetry (DSC) measurements with a TA Instruments model Q200 DSC instrument (with a ramp rate of 10 K/min during heating and cooling) in the temperature range 200–400 K. Magnetic properties of the ribbons were measured in a 9 T Quantum Design PPMS[®] Dynacool[®] platform using the VSM option in a temperature range from 5 K to 400 K. The ribbon samples studied were directly glued to the quartz VSM sample holder using GE-7031 varnish. An external magnetic field was applied along the major length, or rolling direction of the ribbon in order to minimize the internal demagnetizing field. The magnetization versus temperature $M(T)$ curves were measured under low (5 mT) and high (5 T) static fields from 5 to 400 K at a sweep rate of 1.5 K/min.

RESULTS AND DISCUSSION

XRD pattern for $\text{Ni}_{50}\text{Mn}_{35}\text{In}_{14.25}\text{B}_{0.75}$ annealed ribbons measured at room temperature is shown in Figure 1. A mixture of austenite (cubic) and martensite (tetragonal) phases was observed. The XRD pattern of the ribbons is similar to that of bulk Ni-Mn-In based Heusler alloys in the phase coexistence region exhibiting a magnetostructural transition near room temperature.²²

Figure 2(a) shows the zero-field-cooling (ZFC), field-cooling (FC), and field-heating (FH) magnetization $M(T)$ curves in a low external low magnetic field ($\mu_0 H = 5\ \text{mT}$). The thermal protocol followed to measure each magnetization isotherm through the phase transition was as follows: at zero magnetic field the sample was heated to 400 K to stabilize the austenite phase, cooled to 200 K to form

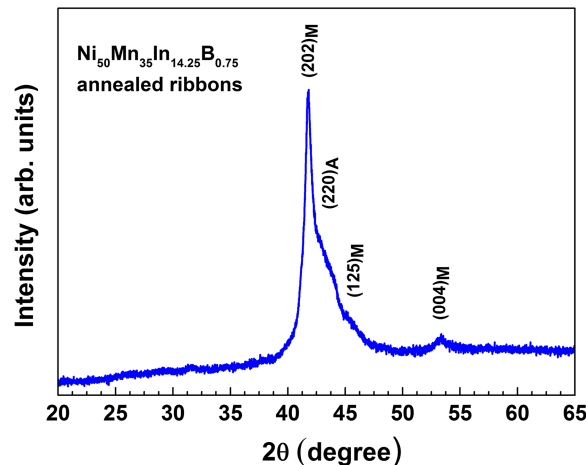


FIG. 1. XRD pattern for a $\text{Ni}_{50}\text{Mn}_{35}\text{In}_{14.25}\text{B}_{0.75}$ annealed ribbons measured at room temperature.

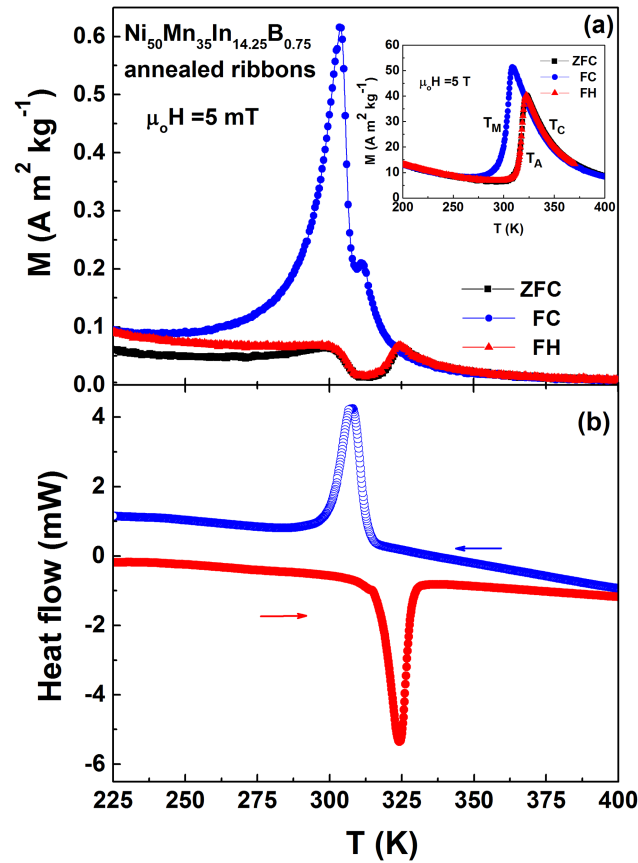


FIG. 2. (a) ZFC, FC, and FH temperature dependent magnetization curves measured under static magnetic fields of 5 mT and 5 T (inset) and (b) DSC heat flow curves as a function of temperature measured on heating (closed symbols) and cooling (open symbols) for $\text{Ni}_{50}\text{Mn}_{35}\text{In}_{14.25}\text{B}_{0.75}$ annealed ribbons.

the martensite, and then heated again in no-overshoot mode to the selected measuring temperature, T_{meas} . This thermal cycling ensures that, prior to apply the magnetic field at a given T_{meas} , the sample assumes the phase constitution that corresponds to the thermally induced structural transition.²³ The presence of thermal hysteresis and the jump-like change in magnetization at the martensitic transition results from the first order nature of the transition. A shift in the martensitic transition by 70 K to higher temperature from $T = 240 \text{ K}$ (bulk value) to $T = 315 \text{ K}$ was observed.²² The inset of Figure 2(a) shows the high field ($\mu_0 H = 5 \text{ T}$) ZFC-FC-FH $M(T)$ curves for annealed ribbons. A sharper and larger difference in the magnetization of about $45 \text{ Am}^2 \text{kg}^{-1}$ was observed at the martensitic transition. The phase transition temperatures have been determined as inflection points of the $M(T)$ curves (from the maximum of the dM/dT curves) obtained during cooling and heating protocols at constant magnetic field. Also from the inset of Figure 2(a), a thermal hysteresis of the MST temperature (T_A and T_M) of about 20 K was observed and found to be smaller than that of the bulks (of about 28 K²²) for a field change of 5 T.

The first order nature of the phase transitions was also confirmed by the temperature hysteresis of the heat flow peaks as shown in Figure 2(b). The temperature hysteresis of the heat flow between heating and cooling cycles detected from DSC measurements is consistent with that measured in the $M(T)$ curves (see Figure 2(a)). The latent heat (L) was estimated for annealed ribbons from their respective endothermic peaks using $L = \int_{A_s}^{A_f} \frac{dQ}{dT} dT$, where $\frac{dQ}{dT}$ is the change in heat flow with temperature, and A_s and A_f are the starting and final temperatures of the reverse martensitic transition, respectively. The latent heat and corresponding total entropy change (ΔS_T) calculated from the DSC curves were found to be 9.81 J/g and 31.5 J/(kgK), respectively. These values of latent heat and entropy changes are similar to those measured for bulk $\text{Ni}_{50}\text{Mn}_{35}\text{In}_{14.25}\text{B}_{0.75}$.²²

Figure 3(a) shows the Arrott plots (M^2 versus $\mu_0 H/M$ plots) for selected temperatures across the martensitic and Curie transition temperatures for $\text{Ni}_{50}\text{Mn}_{35}\text{In}_{14.25}\text{B}_{0.75}$ annealed ribbons. The S-shape curves of the Arrott plots through the magnetostructural transition temperature range confirms the first-order nature of austenitic to martensitic transformation. By plotting M^2 versus $\mu_0 H/M$ plots of the field dependent magnetization ($H = 1/\chi M + \beta M^3 + \gamma M^5 + \dots$), the intercept with the $\mu_0 H/M$ axis when extrapolated to $M^2 = 0$ gives $1/\chi$ and the temperature at which $1/\chi = 0$ is the Curie temperature. Also, the Curie temperature obtained from the Arrott plots across the second-order transition is comparable to the one obtained from the minimum of the dM/dT vs. T curve (see Figure 2(a)). Isothermal magnetization curves $M(\mu_0 H)$ for $\text{Ni}_{50}\text{Mn}_{35}\text{In}_{14.25}\text{B}_{0.75}$ ribbons in the vicinity of the martensitic and Curie transition temperatures are shown in Figure 3(b). The magnetization isotherms were found to show metamagnetic-like behavior at the martensitic transition temperature. At higher temperature, the magnetization curves are characteristic of a transition from ferromagnetic to a paramagnetic state. With increasing temperature, the critical field of the direct metamagnetic transition decreases. Similar behaviors in the $M(\mu_0 H)$ curves were observed for bulk $\text{Ni}_{50}\text{Mn}_{35}\text{In}_{14.25}\text{B}_{0.75}$.²²

The magnetic entropy change (ΔS_M) values were estimated from the isothermal magnetization curves near the martensitic transition using a Maxwell relation.²⁴ Both inverse and direct magnetocaloric effects were observed for bulk and ribbons at the martensitic transition and Curie temperatures, respectively (see Figure 4(a)). The peak values of the magnetic entropy changes $|\Delta S_M^{\text{peak}}|$ in the vicinity of T_M and T_C for $\Delta H = 5\text{T}$ were found to be 16 J/kg K and 4 J/kg K, respectively.

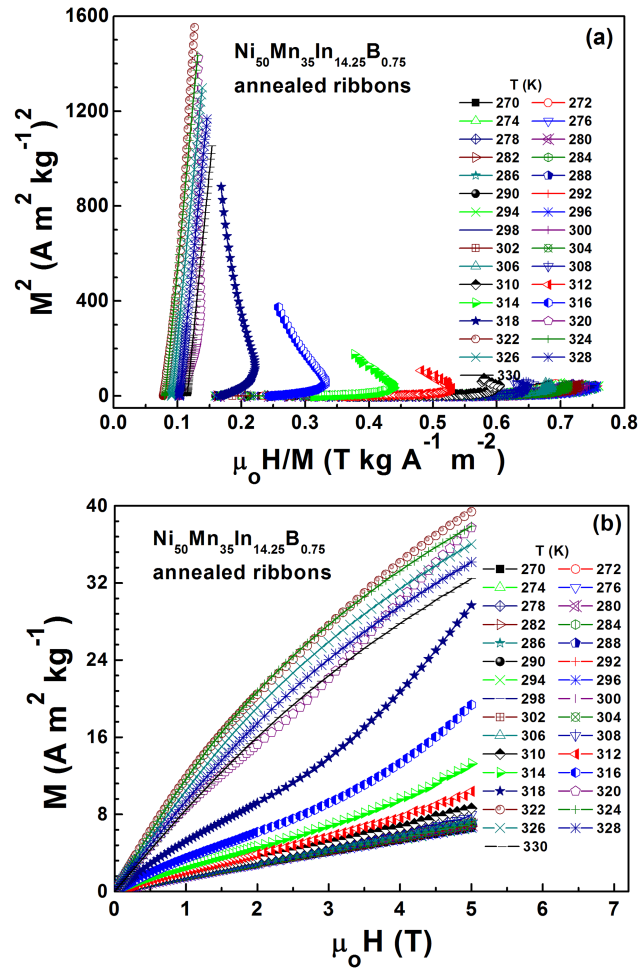


FIG. 3. (a) Arrott plots for selected temperatures across the martensitic and Curie transition temperatures and (b) isothermal magnetization curves measured up to a maximum magnetic field of 5 T for $\text{Ni}_{50}\text{Mn}_{35}\text{In}_{14.25}\text{B}_{0.75}$ annealed ribbons.

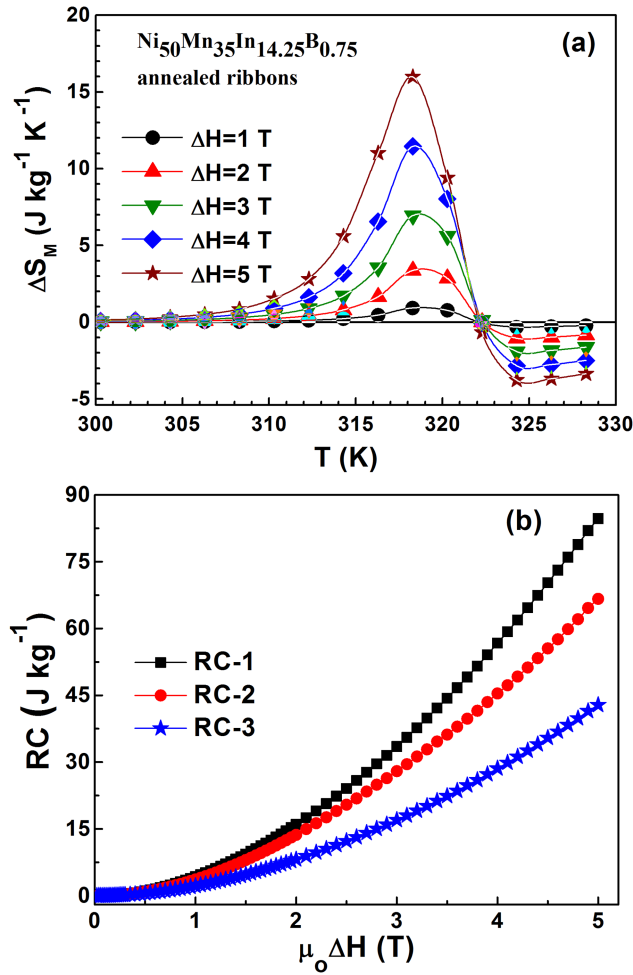


FIG. 4. (a) Temperature (T) and field (H) dependence of the magnetic entropy changes (ΔS_M) and (b) refrigeration capacities RC-1, RC-2, and RC-3 as a function of the magnetic field change for $\text{Ni}_{50}\text{Mn}_{35}\text{In}_{14.25}\text{B}_{0.75}$ annealed ribbons.

The abrupt magnetization change corresponding to the first-order magnetostructural transition leads to an increase of the ΔS_M^{peak} values at T_M in the annealed ribbons relative to those observed in bulk sample ($|\Delta S_M^{\text{peak}}| = 11 \text{ J/kg K}$, for $\Delta H = 5 \text{ T}$ ²²). From the $\Delta S_M(T)$ curves at the martensitic transition, we estimated the Refrigeration capacity (RC) through the following protocols: (a) by calculating the

TABLE I. $|\Delta S_M^{\text{peak}}|$, $RC-1$, $RC-2$, δT_{FWHM} , T_{hot} , T_{cold} , $RC-3$, $\delta T^{\text{RC-3}}$, and $T_{\text{hot}}^{\text{RC-3}}$ and $T_{\text{cold}}^{\text{RC-3}}$ for $\text{Ni}_{50}\text{Mn}_{35}\text{In}_{14.25}\text{B}_{0.75}$ annealed ribbons.

$\mu_0 \Delta H$ (T)	1.0	2.0	3.0	4.0	5.0
$ \Delta S_M^{\text{peak}} $ ($\text{J kg}^{-1} \text{K}^{-1}$)	0.9	3.4	6.9	11.5	16.0
$RC-1$ (J kg^{-1})	4	16	34	57	85
$RC-2$ (J kg^{-1})	4	14	28	45	67
δT_{FWHM} (K)	4.678	4.766	4.829	4.952	5.3
T_{hot} (K)	320.9	321.0	320.9	320.7	320.4
T_{cold} (K)	316.2	316.2	316.1	315.7	315.1
$RC-3$ (J kg^{-1})	2	8	17	29	43
$\delta T^{\text{RC-3}}$ (K)	4.0	4.1	4.2	4.5	4.8
$T_{\text{hot}}^{\text{RC-3}}$ (K) ^a	320.7	320.8	320.7	320.5	320.2
$T_{\text{cold}}^{\text{RC-3}}$ (K) ^a	316.7	316.7	316.5	316.0	315.4

^aRelated to RC-3.

product $|\Delta S_M^{\text{peak}}| \times \delta T_{\text{FWHM}}$ (referred as RC-1), where $\delta T_{\text{FWHM}} = T_{\text{hot}} - T_{\text{cold}}$ corresponds to the full-width at half-maximum of the $\Delta S_M(T)$ curve; (b) by calculating the area under the $\Delta S_M(T)$ curve between T_{hot} and T_{cold} (RC-2); and (c) by maximizing the product $\Delta S_M \times \delta T$ below the $\Delta S_M(T)$ curve (RC-3). The refrigerant capacities, RC-1, RC-2, and RC-3 for $\text{Ni}_{50}\text{Mn}_{35}\text{In}_{14.25}\text{B}_{0.75}$ annealed ribbons as a function of the magnetic field change up to 5 T are shown in Figure 4(b). The RC values and related parameters are given in Table I. This values of RC is comparable to bulk $\text{Ni}_{50}\text{Mn}_{35}\text{In}_{14.25}\text{B}_{0.75}$ systems²² and those of other Ni-Mn-In based Heusler alloys.⁹

CONCLUSIONS

In conclusions, we have investigated the magnetostructural transitions, magnetic, and magnetocaloric properties of $\text{Ni}_{50}\text{Mn}_{35}\text{In}_{14.25}\text{B}_{0.75}$ annealed ribbons. The martensitic transition temperature for annealed ribbons shift by about 70 K to a higher temperature relative to that of the bulk. A sharper martensitic transition resulting in larger magnetic entropy changes was observed for $\text{Ni}_{50}\text{Mn}_{35}\text{In}_{14.25}\text{B}_{0.75}$ annealed ribbons. Most of the parameters related to the magnetic responsive properties of annealed ribbons were found to be larger to those reported for the bulk alloy. This results indicates that the $\text{Ni}_{50}\text{Mn}_{35}\text{In}_{14.25}\text{B}_{0.75}$ annealed ribbons may be promising multifunctional materials.

ACKNOWLEDGMENTS

This work was supported by the Office of Basic Energy Sciences, Material Science Division of the U.S. Department of Energy, DOE Grant No. DE-FG02-06ER46291 (SIU) and DE-FG02-13ER46946 (LSU). The authors acknowledge financial support received from Laboratorio Nacional de Investigaciones en Nanociencias y Nanotecnología (LINAN, IPICYT) and CONACy T, Mexico (Grant No. 286993). The technical support of M.Sc. B.A. Rivera-Escoto is gratefully acknowledged. C.F. Sánchez-Valdés is grateful to DMCU-UACJ for supporting his research exchange with IPICYT (program PFCE and academic mobility grant); also, for the financial support received from CONACYT (Grant No. 286993) and PRODEP-SEP, Mexico.

- ¹ A. O. Pecharsky, K. A. Gschneidner, Jr., and V. K. Pecharsky, *J. Appl. Phys.* **93**, 4722 (2003).
- ² O. Tegus, E. Bruck, K. H. J. Buschow, and F. R. de Boer, *Nature (London)* **415**, 150 (2002).
- ³ T. Krenke, E. Duman, M. Acet, E. F. Wassermann, X. Moya, L. Mañosa, and A. Planes, *Nat. Mater.* **4**, 450 (2005).
- ⁴ M. Khan, A. K. Pathak, M. R. Paudel, I. Dubenko, S. Stadler, and N. Ali, *J. Magn. Magn. Mater.* **320**, L21 (2008).
- ⁵ S. Y. Yu, Z. H. Liu, G. D. Liu, J. L. Chen, Z. X. Cao, G. H. Wu, B. Zhang, and X. X. Zhang, *Appl. Phys. Lett.* **89**, 162503 (2006).
- ⁶ I. Dubenko, A. K. Pathak, S. Stadler, N. Ali, Ya. Kovarskii, V. N. Prudnikov, N. S. Perov, and A. B. Granovsky, *Phys. Rev. B* **80**, 092408 (2009).
- ⁷ K. Ullakko, J. K. Huang, C. Kantner, R. C. O. Handley, and V. V. Kokorin, *Appl. Phys. Lett.* **69**, 1966 (1996).
- ⁸ I. Dubenko, A. Quetz, S. Pandey, A. Aryal, I. Rodionov, V. Prudnikov, E. Lahderanta, T. Samanta, A. Saleheen, S. Stadler, and N. Ali, *J. Magn. Magn. Mater.* **383**, 186–189 (2015).
- ⁹ A. K. Pathak, I. Dubenko, M. Khan, S. Stadler, and N. Ali, *J. Appl. Phys. Lett.* **90**, 262504 (2007).
- ¹⁰ S. Pandey, A. Quetz, A. Aryal, I. Dubenko, T. Samanta, D. Mazumdar, S. Stadler, and N. Ali, *AIP Advances* **6**, 056213 (2016).
- ¹¹ Z. B. Li, J. L. Sánchez Llamazares, C. F. Sánchez-Valdés, Y. D. Zhang, C. Esling, X. Zhao, and L. Zuo, *Appl. Phys. Lett.* **100**, 174102 (2012).
- ¹² J. L. Sánchez Llamazares, H. Flores-Zuñiga, C. Sánchez-Valdes, C. A. Ross, and C. García, *J. Appl. Phys.* **111**, 07A932 (2012).
- ¹³ P. J. Ibarra-Gaytan, C. F. Sánchez-Valdés, J. L. Sánchez Llamazares, P. Álvarez-Alonso, P. Gorria, and J. A. Blanco, *Appl. Phys. Lett.* **103**, 152401 (2013).
- ¹⁴ C. F. Sánchez-Valdés, P. J. Ibarra-Gaytan, J. L. Sánchez Llamazares, M. Avalos-Borja, P. Álvarez-Alonso, P. Gorria, and J. A. Blanco, *Appl. Phys. Lett.* **104**, 212401 (2014).
- ¹⁵ C. F. Sánchez-Valdés, J. L. Sánchez Llamazares, H. Flores-Zuñiga, D. Rios-Jara, P. Alvarez, and P. Gorria, *Scripta Mater.* **69**, 211–214 (2013).
- ¹⁶ A. M. Aliev, A. B. Batdalov, V. V. Koledov, V. G. Shavrov, V. D. Buchelnikov, J. García, V. M. Prida, and B. Hernando, *Appl. Phys. Lett.* **97**, 212505 (2010).
- ¹⁷ Z. Li, C. F. Sanchez Valdes, J. L. Sanchez Llamazares, Y. Zhang, C. Esling, X. Zhao, and L. Zuo, *IEEE Trans. Magn.* **51**, 11 (2015).
- ¹⁸ J. L. Sánchez Llamazares, B. Hernando, C. García, J. González, Ll. Escoda, and J. J. Suñol, *J. Phys. D: Appl. Phys.* **42**, 045002 (2009).
- ¹⁹ H. Zhenga, D. Wua, S. Xuea, J. Frenzlc, G. Eggelerc, and Q. Zhaib, *Acta Materialia* **59**, 5692–5699 (2007).

- ²⁰ S. Pandey, A. Quetz, A. Aryal, D. Mazumdar, I. Dubenko, S. Stadler, and N. Ali, *J. Magn. Magn. Mater.* **444**, 98–101 (2017).
- ²¹ S. Pandey, A. Quetz, A. Aryal, I. Dubenko, D. Mazumdar, S. Stadler, and N. Ali, *J. Appl. Phys.* **121**, 133901 (2017).
- ²² S. Pandey, A. Quetz, A. Aryal, T. Samanta, I. Dubenko, S. Stadler, and N. Ali, *J. Appl. Phys.* **117**, 183905 (2015).
- ²³ A. Quintana-Nedelcos, J. L. Sánchez Llamazares, C. F. Sánchez-Valdés, P. Álvarez Alonso, P. Gorria, P. Shamba, and N. A. Morley, *J. Alloys Compd.* **694**, 1189 (2017).
- ²⁴ A. M. Tishin and Y. I. Spichkin, *The Magnetocaloric Effects and its Applications* (IOP Publishing Ltd, 2003).